Supporting Information for

High Throughput Screening of Novel Tribromide Perovskite Materials for High-Photovoltage Solar Cells

Shi Chen[1, 2, 3†], Lihua Zhang[2, 4†], Yanliang Liu[2†], Zhuoqiong Zhang[5], Yang Li[2], Weizheng Cai[2], Haiyan Lv[2], Yanchun Qin[2], Qianlong Liao[2], Bin Zhou[2], Ting Yan[2], Jie Ren[2], Shuming Chen[6], Xiaodong Xiang[2], Songyuan Dai[7], Shu Kong So[5], Xingzhu Wang[1, 2, *], Shihe Yang[4, 8, *], Baomin Xu[2, *]

[1]Academy for Advanced Interdisciplinary Studies, Southern University of Science and Technology, Shenzhen, Guangdong Province 518055, China

[2]Department of Materials Science and Engineering and Shenzhen Engineering Research and Development Center for Flexible Solar Cells, Southern University of Science and Technology, Shenzhen, Guangdong Province 518055, China

[3]Henan Key Laboratory of Photovoltaic Materials, Henan University, Kaifeng 475004, China

[4]Department of Chemistry, The Hong Kong University of Science and Technology, Clear Water Bay, Kowloon, Hong Kong, China

[5]Department of Physics, Hong Kong Baptist University, Kowloon Tong, Hong Kong, China

[6]Department of Electrical and Electronic Engineering, Southern University of Science and Technology, Shenzhen, Guangdong Province 518055, China

[7]State Key Laboratory of Alternate Electrical Power System with Renewable Energy Sources, North China Electric Power University, Beijing 102206, China

[8]Guangdong Key Lab of Nano-Micro Material Research, School of Chemical Biology and Biotechnology, Shenzhen Graduate School, Peking University, Shenzhen, Guangdong Province 518055, China

*Correspondence should be addressed to Prof. Xingzhu Wang, Prof. Shihe Yang and Prof. Baomin Xu (emails: wangxz@sustech.edu.cn, chsyang@pku.edu.cn, xubm@sustech.edu.cn)

[†]These authors contributed equally to this work.

Experimental section

Materials: Methylammonium bromide (MABr, 99.5%), formamidine bromide (FABr, 99.5%), poly(bis(4-phenyl)(2,4,6-trimethylphenyl)amine) (PTAA, 6000~16000 MW), bathocuproine (BCP), lead bromide ($PbBr_2$, 99.99%) and 4-fluorophenethylammonium iodide (F-PEAI) were purchased from Xi'an Polymer Light Technology Corporation. Cesium bromide (CsBr, 99.9%) was bought from Alfa Aesar. Indene-C_{60} bisadduct (ICBA) was purchased from 1-Material. Solvents including dimethylformamide (DMF, anhydrous 99.8%), dimethyl sulfoxide (DMSO, anhydrous 99.8%), isopropanol and chlorobenzene (CB, anhydrous 99.8%) were purchased from Sigma-Aldrich. Patterned indium tin oxide (ITO) glasses were bought from Advanced Election Technology Co. Ltd.

Ink Preparation: Three perovskite inks were prepared for inkjet printing: $FAPbBr_3$ (0.2 M FABr and 0.2 M $PbBr_2$ in DMF), $MAPbBr_3$ (0.2 M MABr and 0.2 M $PbBr_2$ in DMF), and $CsPbBr_3$ (0.2 M CsBr and 0.2 M $PbBr_2$ in DMSO). For the fabrication of solar cells with a specific composition, the precursor solutions were prepared by dissolving FABr, MABr, and $PbBr_2$ in the corresponding molar ratio in the mixed solvent of DMF and DMSO (2 : 1 in volume) with a molar concentration of 1.0 M.

Inkjet Printing of Mixed Perovskite Films: Glass substrates (15 × 15 mm^2) were ultrasonically cleaned with detergent, deionized water, acetone and isopropanol in sequence for 15 min. The pre-cleaned glass substrates were treated in a UV cleaner for 20 min. Employing three prepared precursors, the mixed perovskite films were inkjet-printed on heated (~60 °C) glass substrates at ambient condition (~25 °C and

~35% relative humidity, cleanroom) with a Jetlab 4 printer (MicroFab Technologies) equipped with a piezoelectric-driven inkjet nozzle (diameter: 50 μm), where the printheads were set as ~40 ◦C. Subsequently, these inkjet-printed films were annealed at 100-150 ℃ for 20 min in air in cleanroom, and the pure $CsPbBr_3$ film was further heated at 250℃ for 5 min. Each jetting droplet volume was set as 100 pL, and the total ejected dots for each mixed perovskite film was fixed at 37500 (500 × 75, 15 × 15 mm^2). The jetting droplet number from each printhead was set according to the mixed perovskite compositions, and each printhead worked along the same printing route with different ejected dots. Compared with films for demonstration (**Figure 1e**, 15 × 15 mm^2), smaller films with an area of 5 × 2 were inkjet-printed for properties characterization.

Solar cell fabrication: ITO substrates (15 × 15 mm^2) were ultrasonically cleaned with detergent, deionized water, acetone and isopropanol in sequence for 15 min. The pre-cleaned ITO substrates were then treated in a UV cleaner for 20 min. PTAA film was first deposited by spin-coating the PTAA solution (0.2 wt% in CB) at 4000 rpm for 30s, followed by an annealing step at 120 ℃ for 10 min. The as-prepared perovskite precursor solution was filtered using 0.45 μm polytetrafluoroethylene (PTFE) syringe filter and then was spin-coated onto the ITO / PTAA substrate at a speed of 5000 rpm for 30 s. During the last 15 s of the spin-coating process, the substrate was quickly treated with drop-casting 100 μL ICBA solution (2 mg/ml in CB). Subsequently, the substrate was dried on a hot plate at 115 ◦C for 20 min. For the perovskite passivation, the F-PEAI solution (2.5 mg/mL in isopropanol) was spin-coated onto the perovskite

surface at 5000 rpm for 30s. ICBA solution (20 mg/mL in CB) was spin-coated at 1200 rpm for 30s over the perovskite layer, followed by spin-coating the BCP solution (0.5 mg/mL in isopropanol) at 4000rpm for 30s. Finally, a 100 nm thick silver counter electrode was deposited through a shadow mask by thermal evaporation under a base pressure of 10^{-4} Pa with a device area of 0.08 cm^2.

Characterization: The X-ray diffraction analysis was performed on a Bruker D8 Discover X-ray diffractometer with Cu Kα radiation (1.54 Å). The absorbance spectra were measured by a UV-Vis-NIR spectrometer equipped with an integrating sphere (PerkinElmer Lambda 750). Photoluminescence (PL) and time-resolved PL spectra were recorded by spectrofluorometer (FLS1000, Edinburgh instruments), and 405 nm pulsed laser was utilized as excitation source for the time-resolved PL measurements. The morphology of perovskite films was characterized by scanning electron microscopy (SEM, TESCAN MIRA3) at a 5 KV accelerating voltage. J-V curves were measured under AM 1.5G one sun illumination (100 mW cm^{-2}) with a solar simulator (Enlitech SS-F7-3A) equipped with a 300 W Xenon lamp and a Keithley 2400 source meter. The light intensity was calibrated by an NREL standard Si solar cell. The external quantum efficiency (EQE) spectra were tested employing an EQE system (Enlitech QE-R3011) including a Xenon lamp, a monochromator, a Si detector for calibration and a dual-channel power. The electrochemical impedance spectroscopy (EIS) measurements were performed employing an impedance analyzer (Zahner PP211) in the dark condition. Transient photovoltage was recorded by Zennium workstation (Zahner) equipped with controlled intensity modulated photo

spectroscopy system.

PDS samples were coated on 1 mm thick quartz substrates (5 mm × 15 mm), and then were immersed in perfluorohexane (FC-72) as the deflection fluid. Monochromatic light was shined on the sample using a 1 kW Xenon arc lamp with a 1/4 m monochromator (Oriel) as the pump beam. The pump beam was modulated at 13 Hz by a mechanical chopper. The signal was probed by directing a HeNe laser (JDSU) parallel to the surface of the sample. A quadrant cell (United Detector Technology) was used as the position sensor for monitoring the photothermal deflection signal of the probe beam. The output of the detector was fed into a lock-in amplifier (Stanford Research, Model SR830) for phase-sensitive measurements. All PDS spectra were normalized to the incident power of the pump beam. The schematic diagram of the experimental setup can be found in the previous work.[1]

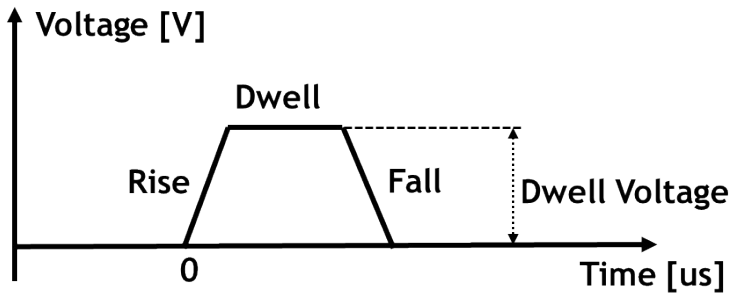

Figure S1 A graphical illustration of the input voltage waveform as a function of time.

Table S1 Summary of time and voltage parameters of the input voltage waveform.

Precursor	Rise Time [us]	Dwell Time [us]	Fall Time [us]	Dwell Voltage [V]
$FAPbBr_3$	2	18 ± 2	16 ± 2	30.0 ± 2.0
$MAPbBr_3$	2	18 ± 2	16 ± 2	30.0 ± 2.0
$CsPbBr_3$	2	15 ± 2	8 ± 2	34.0 ± 2.0

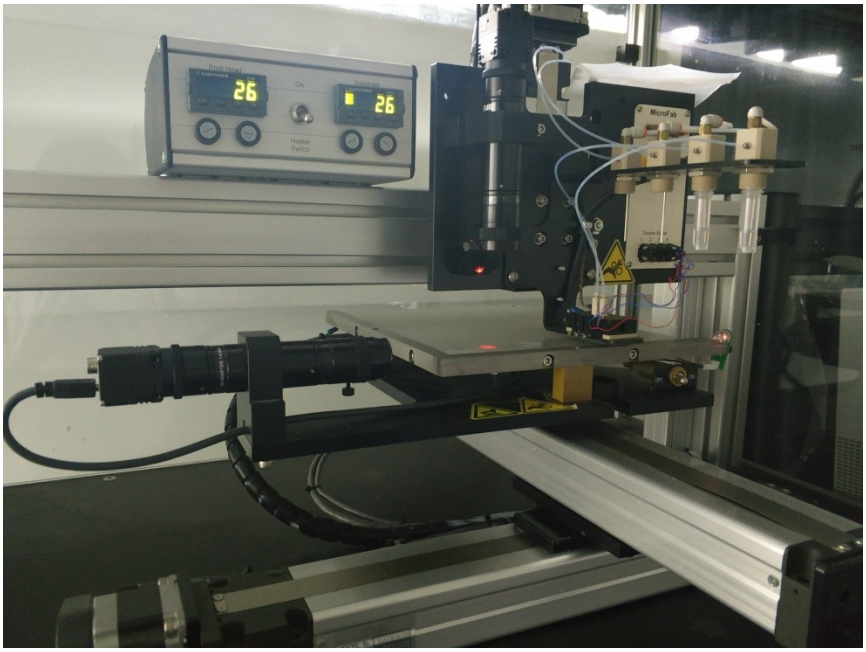

Figure S2 Photograph of the four-channel non-parallel drop-on-demand (DOD) inkjet printer.

Figure S3 A graphical illustration of 30 inkjet-printed mixed films with markings.

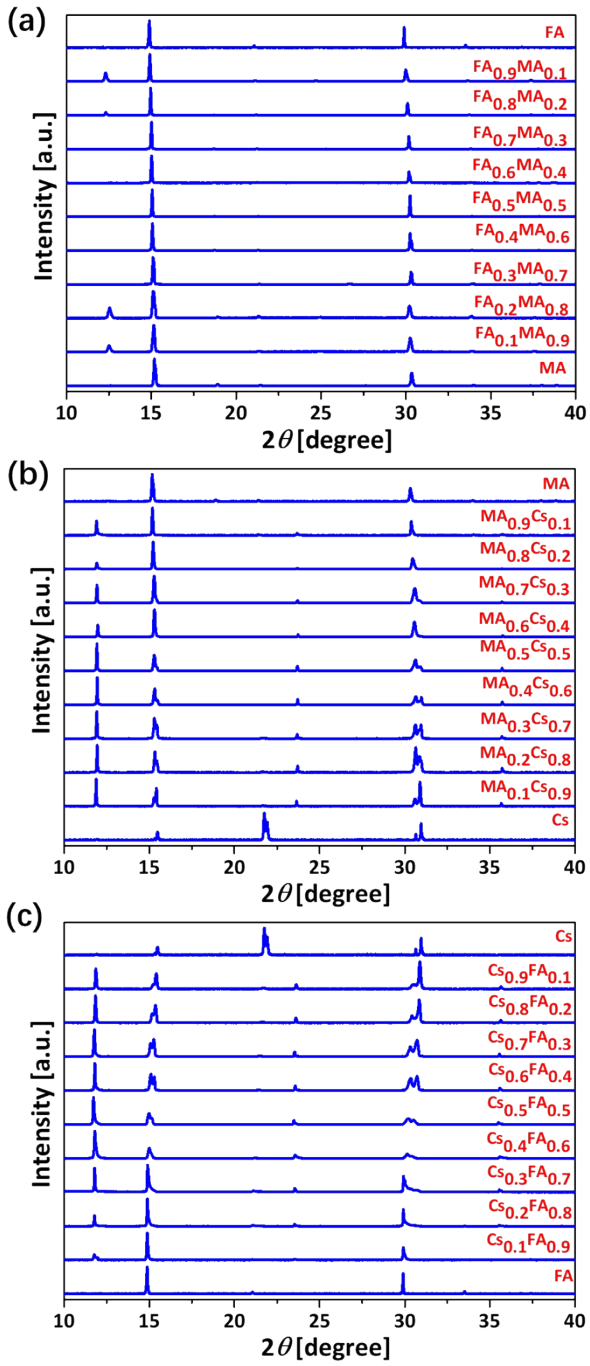

Figure S4 XRD patterns of inkjet-printed $FA_{1-x}MA_xPbBr_3$ (a), $MA_{1-x}Cs_xPbBr_3$ (b) and $Cs_{1-x}FA_xPbBr_3$ (c) thin films.

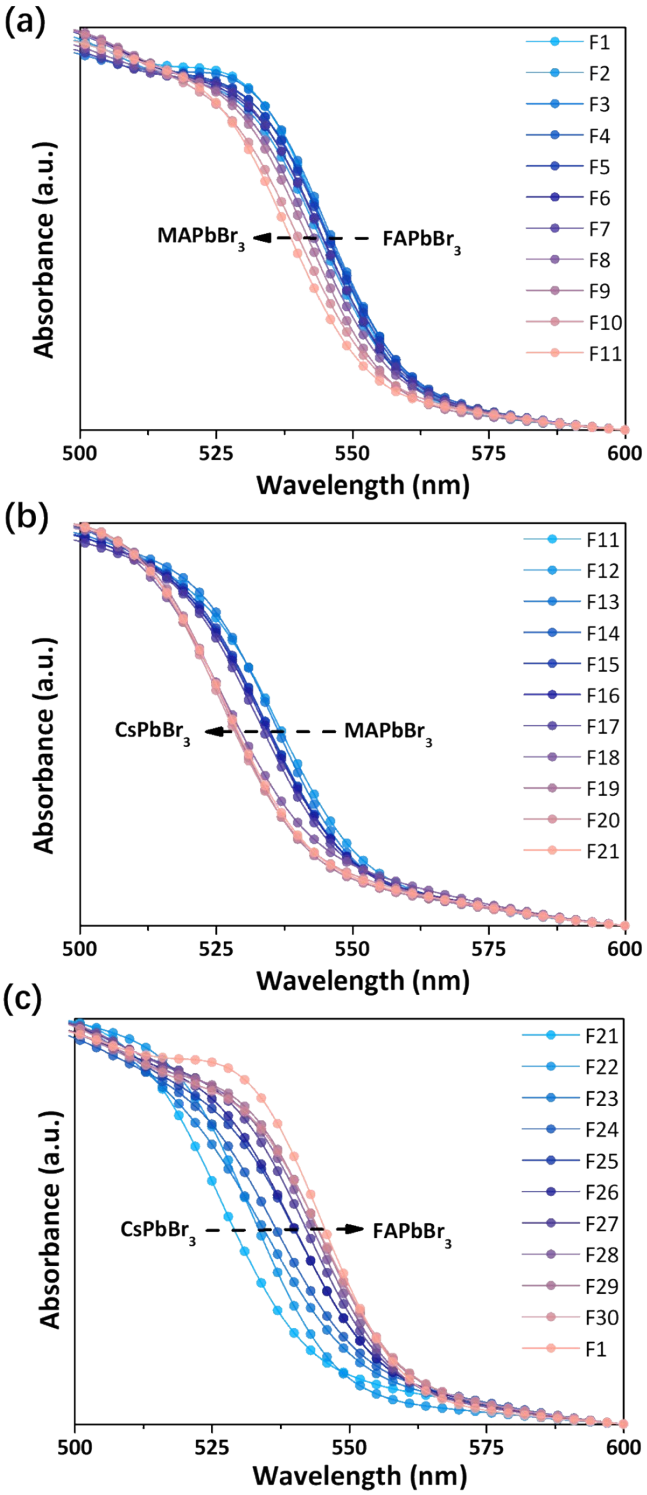

Figure S5 Absorbance spectra of inkjet-printed $FA_{1-x}MA_xPbBr_3$ (a), $MA_{1-x}Cs_xPbBr_3$ (b) and $Cs_{1-x}FA_xPbBr_3$ (c) thin films.

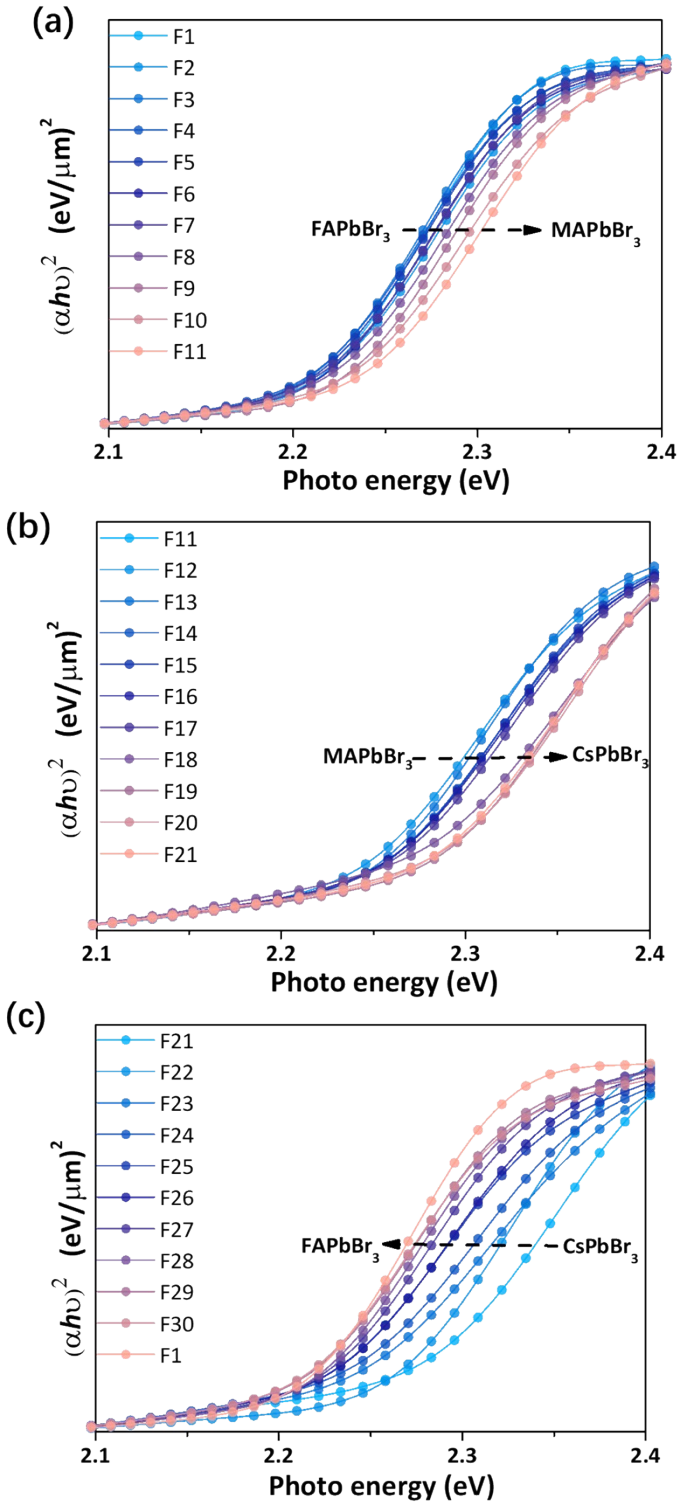

Figure S6 Tauc plots of inkjet-printed $FA_{1-x}MA_xPbBr_3$ (a), $MA_{1-x}Cs_xPbBr_3$ (b) and $Cs_{1-x}FA_xPbBr_3$ (c) thin films.

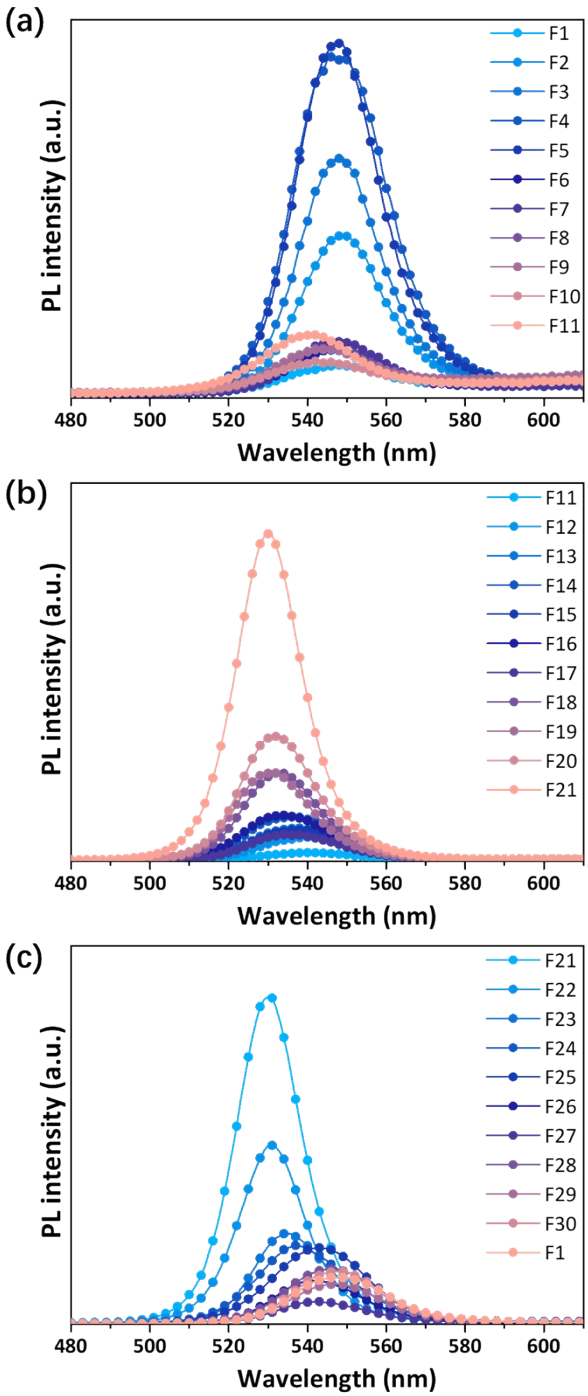

Figure S7 PL spectra of inkjet-printed $FA_{1-x}MA_xPbBr_3$ (a), $MA_{1-x}Cs_xPbBr_3$ (b) and $Cs_{1-x}FA_xPbBr_3$ (c) thin films.

Table S2 Summary of bandgaps, PL peak positions and PL decay lifetimes of 30 inkjet-printed films.

Sample number	E_g [eV]	PL peak position [eV]	τ_1 [ns]	τ_2 [ns]	τ_{ave} [ns]
F1	2.2172	2.2574	0.83	57.0	14.30
F2	2.2181	2.2578	7.17	63.3	26.58
F3	2.2188	2.2601	0.89	35.1	13.58
F4	2.2197	2.2636	0.45	40.3	1.74
F5	2.2201	2.2642	1.48	61.4	20.09
F6	2.2218	2.2668	0.66	90.0	14.80
F7	2.2236	2.2677	0.81	99.5	32.36
F8	2.2265	2.2738	1.31	20.5	5.90
F9	2.2311	2.2772	0.90	23.2	6.68
F10	2.2381	2.2868	0.49	12.9	0.57
F11	2.2433	2.2916	3.05	15.7	6.24
F12	2.2466	2.2944	0.5	24.2	1.00
F13	2.2505	2.3024	0.51	11.2	0.67
F14	2.2536	2.3087	0.56	13.8	0.71
F15	2.2605	2.3097	1.08	15.2	2.28
F16	2.2610	2.3192	1.14	6.49	1.13
F17	2.2634	2.3209	1.54	5.67	2.74
F18	2.2785	2.3270	2.73	10.5	2.34
F19	2.2853	2.3331	0.47	4.75	0.38
F20	2.2878	2.3340	1.46	8.04	1.22
F21	2.2915	2.3386	1.07	4.45	0.81
F22	2.2616	2.3343	1.17	36.0	10.47
F23	2.2482	2.3173	2.4	14.9	4.95
F24	2.2433	2.3090	2.38	14.7	4.88
F25	2.2320	2.2863	2.43	6.25	2.02
F26	2.2311	2.2829	2.62	9.64	3.44
F27	2.2256	2.2778	3.25	9.77	3.07
F28	2.2234	2.2707	3.64	46.5	14.30
F29	2.2192	2.2667	0.79	71.6	18.84
F30	2.2187	2.2626	1.88	53.5	16.19

Table S3 Final Cs / Pb ratios in the $MA_{1-x}Cs_xPbBr_3$ films measured by energy-dispersive X-ray spectrometry.

Film composition	Cs / Pb ratio
$MAPbBr_3$	0
$MA_{0.8}Cs_{0.2}PbBr_3$	0.197
$MA_{0.6}Cs_{0.4}PbBr_3$	0.438
$MA_{0.4}Cs_{0.6}PbBr_3$	0.591
$MA_{0.2}Cs_{0.8}PbBr_3$	0.798
$CsPbBr_3$	1.035

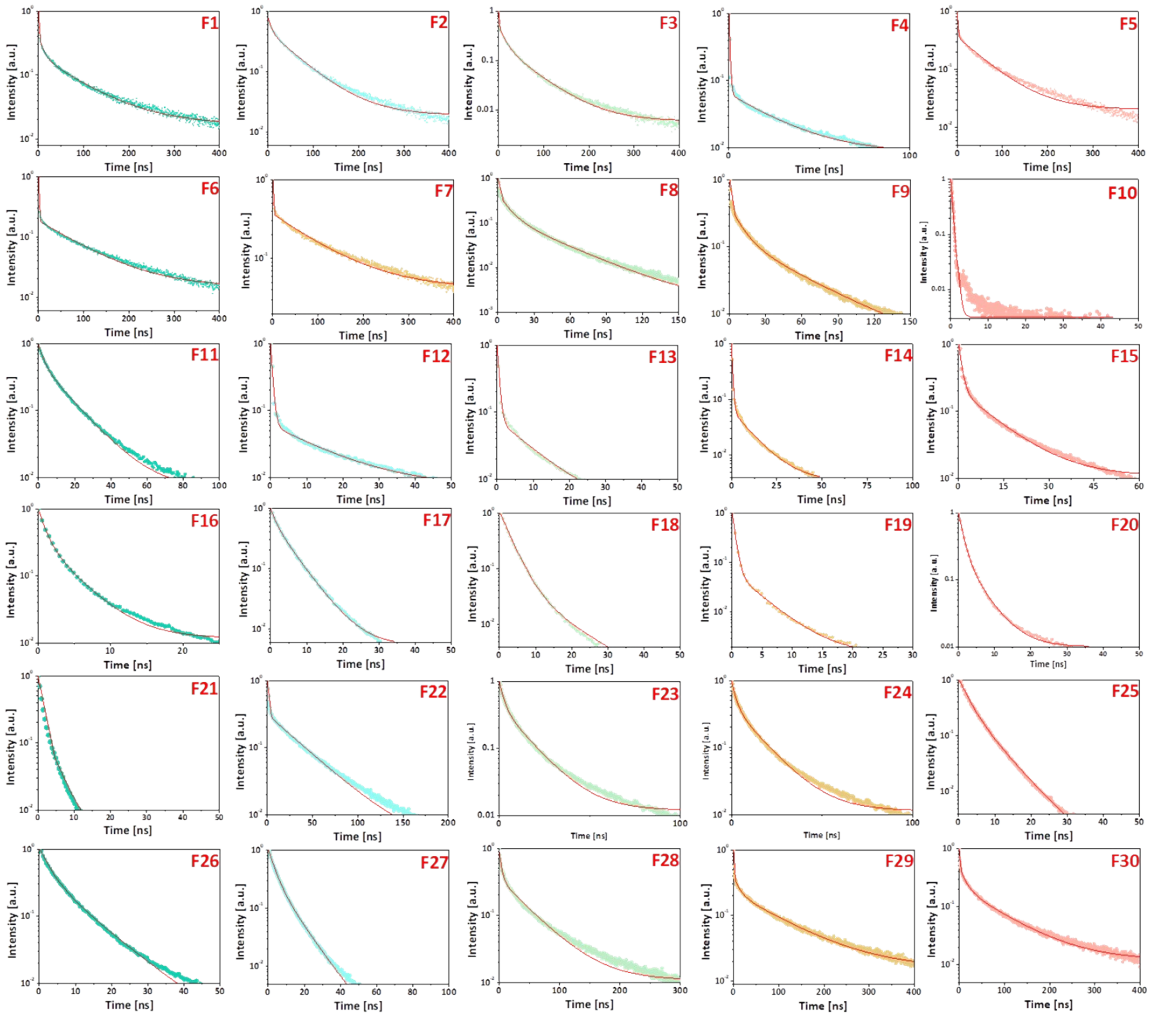

Figure S8 Time-resolved PL spectra of inkjet-printed $FA_{1-x}MA_xPbBr_3$, $MA_{1-x}Cs_xPbBr_3$ and $Cs_{1-x}FA_xPbBr_3$ films on glass substrates.

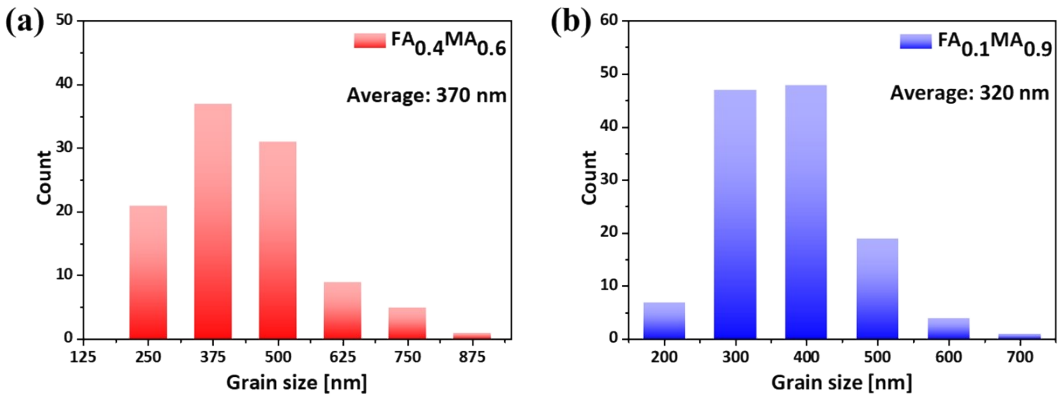

Figure S9 Statistical distributions of the grain size of $FA_{0.4}MA_{0.6}$ (a) and $FA_{0.1}MA_{0.9}$ (b) films coated on PTAA substrates.

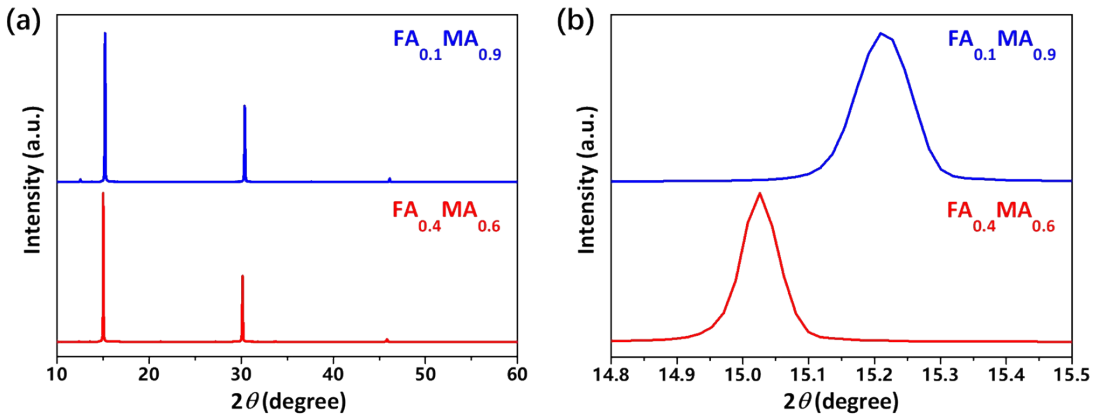

Figure S10 XRD patterns of $FA_{0.4}MA_{0.6}$ and $FA_{0.1}MA_{0.9}$ based films.

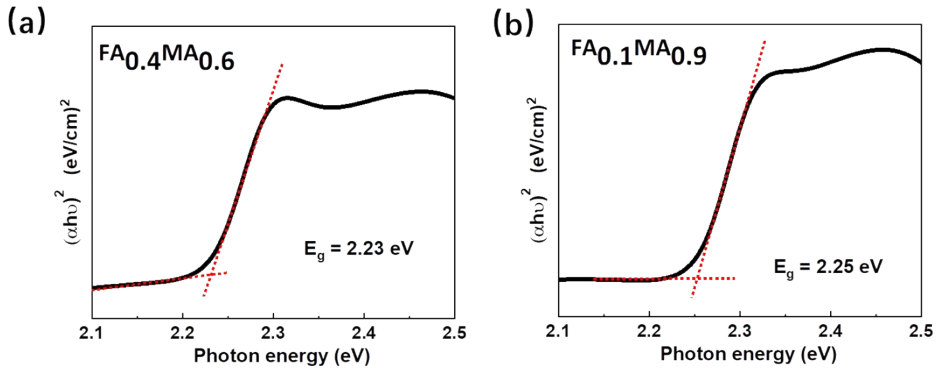

Figure S11 Tauc plots of spin-coated $FA_{0.4}MA_{0.6}$ (a) and $FA_{0.1}MA_{0.9}$ (b) based films.

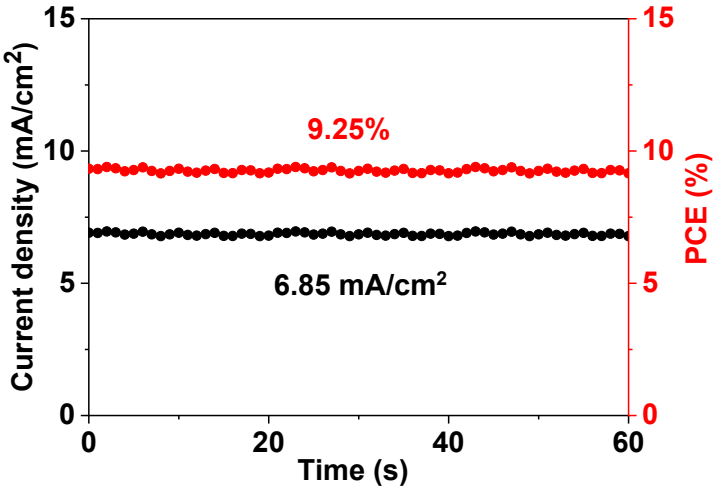

Figure S12 Steady measurement at the maximum power output point of the $FA_{0.4}MA_{0.6}$ champion device.

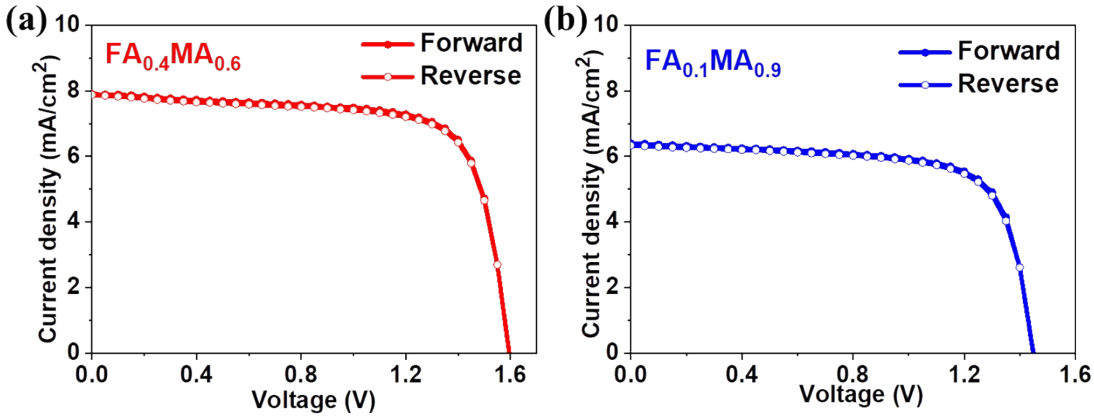

Figure S13 J-V curves of $FA_{0.4}MA_{0.6}$ (a) and $FA_{0.1}MA_{0.9}$ (b) based champion devices at the forward and reverse scan directions.

Table S4 Summary of the reported V_{oc} values for tribromide perovskite solar cells.

Active layer	V_{oc} [V]	Reference
$MAPbBr_3$	1.65	[2]
$FAPbBr_3$	1.51	[3]
$MAPbBr_3$	1.57	[4]
$MAPbBr_3$	1.52	[5]
$CsPbBr_3$	1.62	[6]
$CsPbBr_3$	1.59	[7]
$MAPbBr_3$	1.52	[8]
$MAPbBr_3$	1.53	[9]
$FAPbBr_3$	1.50	[10]
$MAPbBr_3$	1.61	[11]
$MAPbBr_3$	1.51	[12]
$MAPbBr_3$	1.40	[13]
$CsPbBr_3$	1.70	[14]
$CsPbBr_3$	1.702	[15]
$FA_{0.4}MA_{0.6}PbBr_3$	1.60	This work

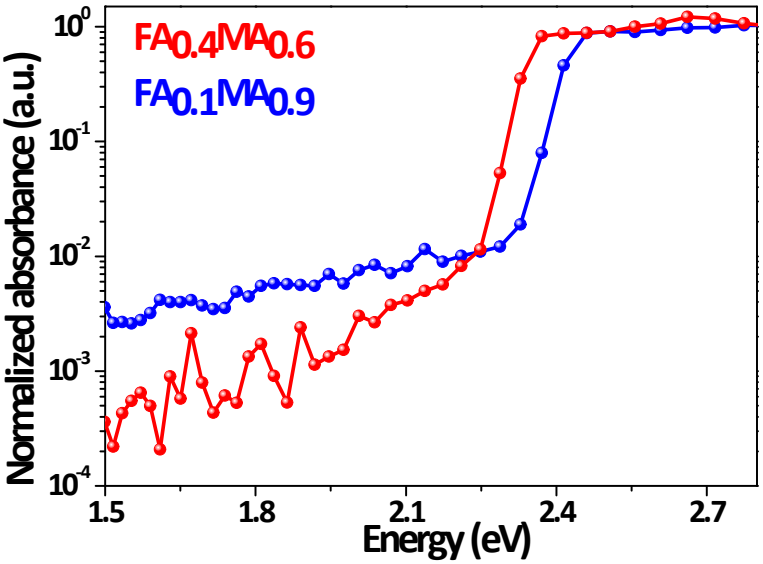

Figure S14 Normalized PDS absorbance spectra of $FA_{0.4}MA_{0.6}$ and $FA_{0.1}MA_{0.9}$ films.

Table S5 Summary of fitting parameters from the time-resolved PL spectra in Figure 6b.

Film	τ_1 [ns]	τ_2 [ns]	τ_{avg} [ns]
$FA_{0.4}MA_{0.6}$	2.98	59.5	37.3
$FA_{0.1}MA_{0.9}$	2.85	27.4	13.5

Calculation of the series resistance (R_s) and the dark saturated current density (J_0)[16, 17]

The classical diode equation in the main text can also be described as:

$$-\frac{dV}{dJ} = \frac{nkT}{q}(J_{sc} - J)^{-1} + R_s \quad \text{(S1)}$$

$$\ln(J_{sc} - J) = \frac{q}{nkT}(V + R_s J) + lnJ_0 \quad \text{(S2)}$$

The J-V curves in **Figure 6b** is used for analysis. By fitting the curves of –dV / dJ versus $(J_{sc} - J)^{-1}$ and ln $(J_{sc} - J)$ versus $(V + R_s J)$ (**Figure 6c-d**), we can obtain R_s and J_0 for solar cells, respectively.

Calculation of the saturation current density for radiative recombination ($J_{0,rad}$)[18, 19]

According to Beer-Lambert's approximation (assuming no reflection):

$$I_A = I_0(1 - e^{-\alpha t}) \quad \text{(S3)}$$

Where I_A stands for the current generated from the absorbed photons, I_0 represent the current generated from incident photons, α denotes the absorption coefficient, and t is the photoactive layer thickness. Highly-sensitive external quantum efficiency (EQE) spectra (**Figure 7a**) can be obtained from absorption spectra measured by photothermal deflection spectroscopy (PDS) (**Figure S14**).

$$EQE = \frac{I_A}{I_0} = 1 - e^{-\alpha t} \quad \text{(S4)}$$

Assuming that all recombination is radiative at the open circuit condition, it is possible to calculate $J_{0,rad}$ based on the photovoltaic EQE spectra.

$$J_{0,rad} = q\int_0^{\infty} EQE(E) \times \emptyset_{bb}(E) \times dE \quad \text{(S5)}$$

Where q is the elementary charge, E is the photon energy and ϕ_{bb} is the spectral photon density of a black body.

To circumvent the noise limitations of EQE spectra at very low, sub-band gap energies, we made use of a reciprocity relation outlined elsewhere to correlate the electroluminescence emission of a photovoltaic device with its quantum efficiency.

$$\emptyset_{EL}(E) = EQE(E) \times \emptyset_{bb}(E) \times [\exp\left(\frac{qV}{kT}\right) - 1] \quad \text{(S6)}$$

ϕ_{EL} is the emitted spectral photon density originating from electroluminescence emission.

1. X. Meng, J. Zhou, J. Hou, X. Tao, S. H. Cheung, S. K. So and S. Yang, *Adv. Mater.*, 2018, **30**, 1706975.
2. X. Hu, X.-F. Jiang, X. Xing, L. Nian, X. Liu, R. Huang, K. Wang, H.-L. Yip and G. Zhou, *Solar RRL*, 2018, **2**, 1800083.
3. Y. Ko, Y. Kim, C. Lee, Y. Kim, B. K. Min, H.-j. Gwon, Y. J. Yun and Y. Jun, *ACS Appl. Energy Mater.*, 2020, **3**, 2331-2341.
4. Y. Liang, Y. Wang, C. Mu, S. Wang, X. Wang, D. Xu and L. Sun, *Adv. Energy Mater.*, 2018, **8**, 1701159.
5. N. K. Noel, B. Wenger, S. N. Habisreutinger, J. B. Patel, T. Crothers, Z. Wang, R. J. Nicholas, M. B. Johnston, L. M. Herz and H. J. Snaith, *ACS Energy Lett.*, 2018, **3**, 1233-1240.
6. Y. Zhao, J. Duan, Y. Wang, X. Yang and Q. Tang, *Nano Energy*, 2020, **67**, 104286.
7. J. Duan, Y. Zhao, X. Yang, Y. Wang, B. He and Q. Tang, *Adv. Energy Mater.*, 2018, **8**, 1802346.
8. C. Zuo and L. Ding, *Adv. Energy Mater.*, 2017, **7**, 1601193.
9. S. Chen, Y. Hou, H. Chen, M. Richter, F. Guo, S. Kahmann, X. Tang, T. Stubhan, H. Zhang, N. Li, N. Gasparini, C. O. R. Quiroz, L. S. Khanzada, G. J. Matt, A. Osvet and C. J. Brabec, *Adv. Energy Mater.*, 2016, **6**, 1600132.
10. N. Arora, S. Orlandi, M. I. Dar, S. Aghazada, G. Jacopin, M. Cavazzini, E. Mosconi, P. Gratia, F. De Angelis, G. Pozzi, M. Graetzel and M. K. Nazeeruddin, *ACS Energy Lett.*, 2016, **1**, 107-112.
11. C.-G. Wu, C.-H. Chiang and S. H. Chang, *Nanoscale*, 2016, 8, 4077-4085.
12. J. H. Heo, D. H. Song and S. H. Im, Adv. Mater., 2014, **26**, 8179-8183.
13. S. Ryu, J. H. Noh, N. J. Jeon, Y. Chan Kim, W. S. Yang, J. Seo and S. I. Seok, *Energy Environ. Sci.*, 2014, **7**, 2614-2618.

14. Q. Zhou, J. Duan, X. Yang, Y. Duan and Q. Tang, *Angew. Chem. Int. Ed.*, 2020, **59**, 21997-22001.
15. Q. Zhou, J. Duan, J. Du, Q. Guo, Q. Zhang, X. Yang, Y. Duan and Q. Tang, *Adv. Sci.*, 2021, 10.1002/advs.202101418.
16. J. You, Y. Yang, Z. Hong, T.-B. Song, L. Meng, Y. Liu, C. Jiang, H. Zhou, W.-H. Chang, G. Li and Y. Yang, *Appl. Phys. Lett.*, 2014, **105**, 183902.
17. J. Shi, J. Dong, S. Lv, Y. Xu, L. Zhu, J. Xiao, X. Xu, H. Wu, D. Li, Y. Luo and Q. Meng, *Appl. Phys. Lett.*, 2014, **104**, 063901.
18. D. Luo, W. Yang, Z. Wang, A. Sadhanala, Q. Hu, R. Su, R. Shivanna, G. F. Trindade, J. F. Watts, Z. Xu, T. Liu, K. Chen, F. Ye, P. Wu, L. Zhao, J. Wu, Y. Tu, Y. Zhang, X. Yang, W. Zhang, R. H. Friend, Q. Gong, H. J. Snaith and R. Zhu, *Science*, 2018, **360**, 1442-1446.
19. T. Kirchartz and U. Rau, *J. Appl. Phys.*, 2007, **102**, 104510.